

NASA TM X-6

DECLASSIFIED-AUTHORITY-MEMO.US:
2313. TAINE TO SHAUKLAS
DATED JUNE 15, 1967

Declassified by authority of NASA
Classification Change Notices No. 112
Dated 6/28/67



TECHNICAL MEMORANDUM

X-6

DESIGN AND EXPERIMENTAL INVESTIGATION OF A HIGH-
WEIGHT-FLOW LOW-PRESSURE-RATIO TURBINE

By Donald A. Petrash, Robert R. Nunamaker
and Charles A. Wasserbauer

Lewis Research Center
Cleveland, Ohio

GPO PRICE \$ _____

CFSTI PRICE(S) \$ _____

Hard copy (HC) 3.00

Microfiche (MF) .65

ff 653 July 65

FACILITY FORM 602

N67-31918

(ACCESSION NUMBER)

(THRU)

32

(PAGES)

TMX-6

(NASA CR OR TMX OR AD NUMBER)

1

(CODE)

28

(CATEGORY)

DOCUMENT TITLE UNCLASSIFIED

NATIONAL AERONAUTICS AND SPACE ADMINISTRATION
WASHINGTON

September 1959

NATIONAL AERONAUTICS AND SPACE ADMINISTRATION

TECHNICAL MEMORANDUM X-6

DESIGN AND EXPERIMENTAL INVESTIGATION OF A HIGH-
WEIGHT-FLOW LOW-PRESSURE-RATIO TURBINE *

By Donald A. Petrash, Robert R. Nunamaker,
and Charles A. Wasserbauer

Declassified by authority of NASA
SUMMARY Classification Change Notices No. 10-
Dated ** 6/22/67

An over-all performance evaluation was conducted on a high-weight-flow, low-pressure-ratio, single-stage turbine for use in a turbojet engine designed for a cruise Mach number of 4.0. Results indicated that at the equivalent design operating point the rating efficiency was essentially the estimated design value of 0.83. The equivalent design weight flow was obtained. At over-all rating pressure ratios above 1.75 the stator choked for 60 to 100 percent of equivalent design speed. At speeds above design speed the rotor controlled the weight flow through the turbine.

INTRODUCTION

An investigation of turbine components suitable for use in the powerplants of several advanced supersonic aircraft is currently being made at the NACA Lewis laboratory. As a part of this program the requirements were investigated of a turbine for use in a low-pressure-ratio turbojet engine designed for a cruise Mach number of 4.0. A study of these requirements revealed that a single-stage turbine having reasonable turbine efficiency might be obtained. Such a turbine will have high-weight-flow per unit turbine frontal area, low specific work output, and a low hub-tip radius ratio.

In order to determine the characteristics of a turbine for the above application, an experimental turbine has been designed. In the design of the turbine-rotor-blade passage the diffusion of the suction-surface velocity was kept to a minimum.

The method used in the aerodynamic design of the turbine together with the results of a cold-air experimental performance investigation are presented herein.

* Title, Unclassified.

The over-all turbine performance was obtained over a range of speed from 60 to 120 percent of the equivalent design rotative speed and a range of rating total-pressure ratio from 1.2 to 1.8. The inlet total temperature and pressure were nominally 80° F and 40 inches of mercury absolute, respectively.

SYMBOLS

A	annular area, sq ft
a_{cr}	critical velocity of sound, ft/sec
c	chord length, ft
D_p	pressure-surface diffusion parameter, $\frac{\text{fblade-inlet relative velocity} - (\text{min. blade-surface relative velocity})}{(\text{blade-inlet relative velocity})}$
D_s	suction-surface diffusion parameter, $\frac{(\text{max. blade-surface relative velocity}) - (\text{blade-outlet relative velocity})}{(\text{max. blade-surface relative velocity})}$
D_{tot}	sum of suction- and pressure-surface diffusion parameter, $D_p + D_s$
E	specific work output (based on measured torque), Btu/lb
g	gravitational constant, 32.17 ft/sec ²
N	rotational speed, rpm
p	absolute pressure, lb/sq ft
Q	torque, ft-lb
R	gas constant, 53.35 ft-lb/(lb)(°R)
r	radius, ft
s	blade spacing, ft
T	temperature, °R
U	blade velocity, ft/sec

- V absolute gas velocity, ft/sec
 v relative gas velocity, ft/sec
 w weight flow, lb/sec
 α absolute gas-flow angle measured from axial direction, deg
 β relative gas-flow angle measured from axial direction, deg
 γ ratio of specific heats
 δ ratio of inlet total pressure to NACA standard sea-level pressure of 2116 lb/sq ft
 E function of $\gamma, \frac{\gamma_{s2}}{\gamma} \frac{\left(\frac{\gamma+1}{2}\right)^{\frac{\gamma-1}{\gamma}}}{\frac{\gamma_{sl}}{\left(\frac{\gamma_{sl}+1}{2}\right)^{\frac{\gamma_{sl}-1}{\gamma_{sl}}}}$
 η aerodynamic efficiency, ratio of actual turbine work (based on torque measurements) to ideal turbine work (based on exit pressure p'_3)
 η_x rating efficiency, ratio of actual turbine work (based on torque measurements) to ideal turbine work (based on exit pressure $p'_{x,3}$)
 θ_{cr} squared ratio of critical velocity to critical velocity at NACA standard sea-level temperature of 518.7° R
 ρ gas density, lb/cu ft
 σ blade solidity based on axial chord
 ϕ coefficient of aerodynamic loading

Subscripts :

- e exit
 in inlet
 P pressure surface
 r any radius

s	suction surface
s _l	NACA standard sea-level conditions
t	tip
tot	total
u	tangential
x	axial
0,1,2,3	measuring stations, see fig. 6

Superscripts:

'	total or stagnation state
"	relative total or stagnation state

TURBINE DESIGN

Requirements

It was desired to design a turbine having high-weight-flow per unit frontal area with relatively low specific work output while at the same time maintaining good aerodynamic efficiency.

The cold-air, single-stage turbine used in this investigation is 16 inches in diameter and has a constant hub-tip radius ratio of 0.53. The over-all design requirements for this turbine are as follows:

Equivalent specific work output, E/θ_{cr} , Btu/lb	12.22
Equivalent weight flow, $\frac{w\sqrt{\theta_{cr}}}{\delta}$, ϵ , $\frac{lb}{sec}$	28.09
Equivalent blade-tip speed, $U_t/\sqrt{\theta_{cr}}$, ft/sec	520

These design criterion were selected as a result of an unpublished analysis of a hypothetical turbojet engine designed for a cruise Mach number of 4.0.

Velocity Diagrams

The design velocity diagrams at the free-stream stations at the stator inlet, stator exit, and rotor exit were determined on the basis of the following assumptions: free-vortex flow, simplified radial equilibrium, and over-all adiabatic efficiency of 0.83. These velocity diagrams, and those calculated for stations in the plane of the blade trailing edge for both the stator and rotor, are presented in figure 1. The velocity diagrams and the design efficiency were obtained by an iterative process in which a set of velocity diagrams was calculated based on an assumed efficiency. Using these velocity diagrams, the losses through the turbine were obtained from the average velocity level by the method derived in reference 1. A value of the kinetic-energy loss coefficient λ of 0.06 for the stator and 0.17 for the rotor are used in equation (A6) of reference 1. These values of λ are representative values for low-loss turbines investigated at the Lewis laboratory. A new turbine efficiency was then calculated and compared with the assumed value. This process was continued until the assumed efficiency was within 1 percent of the calculated value. The resulting value of 0.83 for the estimated design efficiency is a reasonable value for the subject turbine. Even though the losses through the turbine are low, the high weight flow resulting in high axial Mach numbers and the low specific work output are not conducive to achieving high efficiency values.

A condition of impulse, defined herein as the rotor relative inlet-critical-velocity ratio equal to the relative exit-critical-velocity ratio in the plane of the trailing edge, exists at the hub of the rotor (see fig. 1).

The energy loss caused by the whirl component of the absolute velocity at the rotor-exit mean section (station 3) amounts to 2.0 percent of the design work output.

These velocity diagrams show that, because of the relatively low radius ratio (0.53) and free-vortex design, a rather wide variation occurs in the flow conditions from hub to tip in both the stator and rotor. For example, the critical velocity ratio $(V/a_{cr})_2$ at the stator exit varies from a supersonic value (1.048) at the hub to 0.698 at the tip section. The turning through the rotor varies from 84.44° at the hub to 40.15° at the tip section. The relative rotor-inlet flow angle β_2 varies from 52.9° at the hub to -2.06° at the tip section. Thus, considerable twist is required in the rotor blade from the hub to the tip sections.

Blade Design

A minimization of blade loss is desired in the design of turbine stator and rotor blades. For a given aspect ratio this can be accomplished by optimizing the solidity. The method of the appendix was used to obtain the initial value of stator- and rotor-blade solidities at the hub, mean, and tip sections for the subject turbine. A blade-loading coefficient ϕ of 0.8 was used in equation (A5) of the appendix and was assumed to be constant over the blade height. The number of blades was determined from the solidities obtained from the appendix, the aspect ratio (3.0), and the turbine radius ratio (0.53).

Simplified radial equilibrium was assumed to exist along radial elements at each axial location through the blade passage. The total-pressure drop through the blade row was assumed to be linear in the axial direction.

Procedure. - In general, the three-dimensional design procedure of reference 2 was used to design the subject turbine stator- and rotor-blade profiles. An outline of the procedure used herein is presented since it differs somewhat from that presented in reference 2.

1. A blade shape was approximated.

- (a) A straight suction surface was drawn from the throat to the trailing edge at the exit flow angle relative to the blade in the plane of the trailing edge at the hub, mean, and tip sections.
- (b) The suction surface at the leading edge was drawn at an angle equal to or slightly less than the inlet relative flow angle at each section.
- (c) The channel shapes were then drawn in such a way that a smooth channel with no abrupt changes in curvature resulted. For the stator the contours were chosen so that a large portion of the turning would occur near the blade leading edge where the flow has low momentum.
- (d) The positions of the velocity potential lines and midchannel streamlines were estimated.

2. In order to obtain a reasonable midchannel velocity distribution at the hub as a first trial, the velocity over the suction surface was assumed constant and equal to the blade-outlet velocity, and the method of appendix B, reference 3, was applied.

3. By using the midchannel velocity distribution at the hub and the radial equilibrium relation of appendix B, reference 3, the blade shape was analyzed to obtain the midchannel and surface-velocity distributions at the hub, mean, and tip sections. The blade speed term in equation (B1) of appendix B, reference 3, is set equal to zero for the stator.

4. The weight flow was then calculated at each axial station through the blade passage using the method of reference 4. If this calculated value of weight flow differed from the design value at any axial station, the midchannel velocity distribution at the hub was altered and the procedure (beginning at step 3) was repeated until the calculated value of weight flow was within one-half of 1 percent of the design value.

5. The suction-surface diffusion was calculated at the three sections. If the diffusion at any section was higher than desired, the blade shape was altered and steps 3 and 4 repeated until a satisfactory blade shape was obtained.

Discussion of stator blade. - The stator-blade solidities obtained by the method of the appendix were calculated assuming zero suction-surface diffusion and a pressure-surface diffusion of 0.55 at the hub, mean, and tip. These solidities resulted in a large increase in axial chord from hub to tip blade sections and relatively high suction-surface diffusion at the hub and mean sections. In order to reduce the suction-surface diffusion at these sections, the axial chord at the hub and mean sections was increased. The final axial chord at the hub is about one-half of that at the tip. The final stator-blade solidities and the resulting values of suction-surface diffusion at the hub, mean, and tip sections are given in table I. Thirty-nine stator blades were used for the subject turbine. The design velocity distributions on the midchannel line and the blade surfaces at the hub, mean, and tip sections are shown in figure 3(a). The pressure-surface diffusion for the stator was not calculated since the velocity at the blade leading edge is not obtainable because of limitations of the stream-filament technique.

The final blade shapes were obtained by stacking the hub, mean, and tip blade profiles so that the midpoints of the potential lines across the channel exits at the three sections were on a radial line. The stator-blade-section profiles are shown in figure 2. The coordinates of the stator-blade sections are presented in table II(a).

Discussion of rotor blade. - The values of rotor-blade surface diffusion used in the method of the appendix to calculate the solidity were zero and 0.55 for the suction and pressure surfaces, respectively, for all three blade sections. The values of solidity and the resulting surface diffusion for the rotor are given in table I. The design requirement of zero suction-surface diffusion has been well satisfied with zero being obtained on the hub and tip sections and 0.10 on the mean section.

The values of pressure-surface diffusion obtained on the hub, mean, and tip sections were 0.50, 0.43, and 0.22, respectively. The velocity distributions on the midchannel line and the blade surfaces at the hub, mean, and tip sections are presented in figure 3(b). Fifty-six blades were used in the rotor. The rotor aspect ratio was three.

The final blade shape was obtained by stacking the hub, mean, and tip section profiles so that the centers of gravity at the three sections were on a radial line in order to minimize the bending stress. The rotor-blade section profiles are shown in figure 2. The coordinates of the rotor-blade sections are presented in table II(b).

APPARATUS

Test Installation

The experimental setup of the turbine is shown in figure 4. The air supply was throttled to the desired turbine-inlet pressure. After throttling, the air weight flow was measured by a submerged, calibrated ASME flange-tap, flat-plate orifice. The air then passed through a filter and into an inlet plenum. Within the inlet plenum, the air passed through a screen and then was directed through a bellmouth, which supplied air to the turbine-stator assembly. The air passed through the turbine into an exhaust plenum, from which it was discharged into the laboratory exhaust facilities.

A single 1700-horsepower cradled dynamometer of the eddy-current dry-gap type was used to absorb the power output of the turbine. The turbine torque output was measured by means of a balanced-diaphragm thrustmeter. The turbine rotative speed was measured with an electronic events-per-unit time meter.

The turbine-stator and -rotor assemblies are shown in figure 5. The turbine rotor-blade design resulted in a blade that was long and thin. Aluminum was used in the fabrication of these blades. Therefore, the final rotor-blade assembly might vibrate excessively during operation to cause blade failure. Structural stability was maintained therefore by first threading a 0.016-inch-diameter stainless steel wire through, then looping it around each rotor blade near the trailing edge in the tip region, (see fig. 5(b)).

Instrumentation

The instrumentation used for the over-all performance evaluation of the turbine was located at stations 0, 1, 2, and 3 as shown in figure 6.

The flow conditions at the turbine inlet were measured by means of two total-temperature probes and two total-pressure probes located in the inlet-plenum chamber (station 0). Static-pressure measurements at stations 1, 2, and 3 were obtained from four wall static taps located on both the inner and outer wall of each measuring station.

The static-pressure taps at stations 1 and 2 were located approximately midway circumferentially between adjacent stator blades. Two total-temperature rakes were located at station 3; each rake consisted of five thermocouples positioned so that the temperatures at the centers of 10 equal annular areas were obtained.

Radial surveys of flow angle were made at station 3 with an angle survey probe mounted in a remotely controlled moveable actuator. A schematic diagram of the axial measuring stations and instrument location at each station is shown in figure 6. Photographs of the instruments are shown in figure 7.

METHODS AND PROCEDURE:

Experimental Procedure

The turbine was operated with a measured inlet total pressure p'_0 of approximately 40 inches of mercury absolute and a nominal inlet total temperature T'_0 of 540°R for rotative speeds of 60- to 120-percent equivalent design speed in 10-percent increments over a range of rating pressure ratio $p'_1/p'_{x,3}$ from 1.2 to 1.8.

Experimental Data Reduction and Performance Calculations

In order to evaluate the over-all turbine performance, calculated values of total pressure at stations 1 and 3 were used. The following one-dimensional equation for obtaining this pressure was derived from the equations of continuity and energy, the equation of state, and the isentropic relation between pressure and temperature.

$$p' = p \left[\frac{1}{2} + \frac{1}{2} \sqrt{1 + \frac{2(r-1)}{r} \frac{R}{g} \left(\frac{w\sqrt{T'}}{pA} \right)^2 \frac{1}{\cos^2 \alpha}} \right] \frac{r}{r-1} \quad (1)$$

The static pressure used in this equation is the numerical average of hub and tip static pressures measured by the wall static-pressure taps at the axial station under consideration. The total temperature is determined by averaging the probe total-temperature readings (corrected

for Mach number) at either station 0 or station 3. Temperature measurements at station 0 were used in the total-pressure computation at station 1. A faired flow-angle measurement is used in equation (1). The radial flow-angle measurements at station 3 were averaged across the annulus, then plotted and faired against the static pressures at this station. The flow direction at station 1 is assumed axial.

In addition to this total-pressure computation at measuring stations 1 and 3, a calculated turbine rating total pressure was computed at the turbine exit (station 3). This rating total pressure is defined as the static pressure at that station plus the pressure corresponding to the axial component of velocity. This rating total pressure can be stated in equation form as:

$$p'_x = p \left(1 + \frac{\gamma - 1}{2} M_x^2 \right)^{\frac{\gamma}{\gamma - 1}} \quad (2)$$

where M_x is the axial component of the one-dimensional annulus Mach number. The ideal equivalent work of the turbine was based on the outlet total pressure, the inlet total pressure, and the inlet total temperature. The actual equivalent work was determined from torque, speed, and weight-flow measurements.

The experimentally obtained equivalent torque and weight-flow data were plotted and faired against the over-all rating total-pressure ratio $p'_1/p'_{x,3}$ for constant values of equivalent blade speed. Information taken from the faired curves of torque and weight flow at even increments of the rating pressure ratio was used to compute the performance map.

RESULTS AND DISCUSSION

The over-all performance of the turbine is presented in figure 8(a) where equivalent work output is plotted against the weight-flow parameter $\frac{WN}{606}$ & for constant values of equivalent speed and rating pressure ratio $p'_1/p'_{x,3}$. In addition, contours of constant brake internal rating efficiency η_x based on $p'_1/p'_{x,3}$ are shown.

At equivalent design work and speed, an efficiency of 0.828 was obtained at a rating pressure ratio of 1.55. Values of efficiency greater than 0.86 were obtained at low-speed turbine operation. Figure 8(a) shows that the turbine yields good efficiency over a wide range of rating pressure ratio and speed.

In order to present a more complete evaluation of the turbine performance, a performance map with the efficiencies of the turbine based on the over-all pressure ratio p_1'/p_3' is presented in figure 8(b).

At equivalent design work output and speed, an efficiency of 0.835 is now obtained at a p_1'/p_3' slightly less than 1.55. This efficiency is only 0.007 higher than the efficiency based on $p_1'/p_{x,3}'$. This small difference in efficiency based on p_1'/p_3' and $p_1'/p_{x,3}'$ shows that the tangential velocities at the turbine outlet are small which indicates a relatively small energy loss due to the exit tangential velocity.

The variation of equivalent weight flow with rating pressure ratio for the equivalent speeds investigated is shown in figure 9. The value for equivalent design weight flow is indicated on the weight-flow ordinate. At equivalent design speed and a rating pressure ratio of 1.55 corresponding to equivalent design work, the measured turbine weight flow was essentially the design value. Choking weight flow, indicated when the curves have a zero slope, was obtained above a rating total-pressure ratio of 1.75 for all speeds investigated. Figure 9 shows that the value of choking weight flow remains constant for speeds up to and including design speed, indicating that the stator choked for these speeds prior to the rotor and controlled the weight flow passed by the turbine. At turbine rotor speeds greater than design the value of choking weight flow decreases, indicating that the rotor blade row chokes initially and limits the turbine weight flow.

The variation of equivalent torque with rating pressure ratio for the equivalent speeds investigated is shown in figure 10. Pressure ratios across the turbine large enough to achieve limiting loading were not obtainable. Limiting loading for any given speed is defined herein as the point at which a further increase in pressure ratio does not produce an increase in torque.

SUMMARY OF RESULTS

The following results were obtained from an experimental investigation of a high-weight-flow, low-pressure-ratio, single-stage turbine. The turbine was operated over a range of equivalent speed and pressure ratio at inlet conditions of 40 inches of mercury absolute and 80° F.

1. At equivalent design work and speed, design weight flow was obtained. The rating efficiency at this point was essentially the estimated design value of 0.83.

2. Over the range of pressure ratio investigated limiting loading was not reached.

3. The stator choked at over-all pressure ratios above 1.75 for 60 to 100 percent of equivalent design speed. At speeds above design the rotor controlled the weight **flow** through the turbine.

Lewis Flight Propulsion Laboratory
National Advisory Committee **for** Aeronautics
Cleveland, Ohio, August 18, 1958

APPENDIX - A METHOD FOR INITIAL EVALUATION OF BLADE SOLIDITY FOR GIVEN BLADE-SURFACE-DIFFUSION PARAMETERS

In order to obtain an initial value of solidity for use in the design of a blade section, a blade-loading coefficient is used similar to that developed in reference 5. The blade-loading coefficient is the ratio of the actual blade loading to an ideal blade loading. In the derivation of reference 5 the ideal blade-loading condition is one in which the inlet stagnation pressure is effective over the entire blade pressure surface while the blade outlet static pressure is effective over the entire suction surface. In the present analysis, also, constant values of velocity and, therefore, static pressure, are assumed on each of the blade surfaces in determining the ideal blade loading. However, the constant surface velocities are determined from the velocity diagrams and assumed values for the blade-surface-diffusion parameters in the present analysis. In addition, the isentropic compressible flow relations are used whereas the method of reference 5 assumes incompressible flow.

The constant suction- and pressure-surface critical velocity ratios for the ideal blade loading are obtained from the relations

$$\left(\frac{V}{a'_{cr}}\right)_{s,r} = \frac{\left(\frac{V}{a'_{cr}}\right)_{e,r}}{(1 - D_{s,r})} \quad (A1)$$

$$\left(\frac{V}{a'_{cr}}\right)_{p,r} = \left(\frac{V}{a'_{cr}}\right)_{in,r} (1 - D_{p,r}) \quad (A2)$$

The corresponding static pressures and densities are obtained from the isentropic-flow relations. The equation for conservation of momentum in the tangential direction for the mass of fluid included in a blade channel may be written

$$c_{x,r} \phi g(p_{p,r} - p_{s,r}) = s_r (\rho V_x)_{i,r} (V_u)_{i,r} - (\rho V_x)_{e,r} (V_u)_{e,r} \quad (A3)$$

Equation (A3) defines the blade-loading coefficient ϕ . Assuming no loss through a blade row,

$$\rho'_i (a'_{cr,i})^2 = \rho'_e (a'_{cr,e})^2$$

Division of equation (A3) by this quantity gives

$$c_{x,r} \phi \left(\frac{p_{p,r} - p_{s,r}}{p_i^*} \right) \left[\frac{p_{ig}^*}{\rho_i^* (a_{cr,i}^*)^2} \right] = s_r \left[\left(\frac{\rho V_x}{\rho^* a_{cr}^*} \right)_{i,r} \left(\frac{V_u}{a_{cr}^*} \right)_{i,r} - \left(\frac{\rho V_x}{\rho^* a_{cr}^*} \right)_{e,r} \left(\frac{V_u}{a_{cr}^*} \right)_{e,r} \right] \quad (A4)$$

With the relations

$$V_x = V \cos a$$

$$V_u = V \sin a$$

the definition of critical velocity, and the perfect gas law, equation (A4) may be solved for solidity to yield

$$\frac{c_{x,r}}{s_r} = \frac{1}{\phi} \frac{\left[\left(\frac{\rho V}{\rho^* a_{cr}^*} \right)_{i,r} \cos \alpha_{i,r} \sin \alpha_{i,r} \right] - \left[\left(\frac{\rho V}{\rho^* a_{cr}^*} \right)_{e,r} \cos \alpha_{e,r} \sin \alpha_{e,r} \right]}{\frac{\gamma + 1}{2\gamma} \left[\left(\frac{p}{p^*} \right)_{p,r} - \left(\frac{p}{p^*} \right)_{s,r} \right]} \quad (A5)$$

Relation (A5) was written with the stator angle a . The same relation may be applied to the rotor by replacing the stator angles a by the flow angles relative to the rotor β . A value of the loading coefficient ϕ of 0.80 has yielded satisfactory values of solidity for use in the initial layout of a blade design.

REFERENCES

1. Forrette, Robert E., Holeski, Donald E., and Plohr, Henry W.: Investigation of the Effects of Low Reynolds Number on the Performance of a Single-Stage Turbine with a Downstream Stator. NASA TM X-9, 1959.
2. Nusbaum, William J., Wasserbauer, Charles A., and Hauser, Cavour H.: Experimental Investigation of a High Subsonic Mach Number Turbine Having a 40-Blade Rotor with Zero Suction-Surface Diffusion. NACA RM E57J22, 1958.

3. Stewart, Warner L., Wong, Robert Y., and Evans, David G.: Design and Experimental Investigation of Transonic Turbine with Slight Negative Reaction Across Rotor Hub. NACA RM E53L29a, 1954.
4. Miser, James W., Stewart, Warner L., and Monroe, Daniel E.: Effect of **High** Rotor Pressure-Surface Diffusion on Performance of a Transonic Turbine. NACA RM E55H29a, 1955.
5. Zweifel, O.: Optimum Blade Pitch **for** Turbo-Machines with Special Reference to Blades of Great Curvature. The Eng. Digest, vol. 7, **no. 11**, Nov. 1946, pp. 358-360; cont., vol. 7, no. 12, Dec. 1946, pp. 381-383.

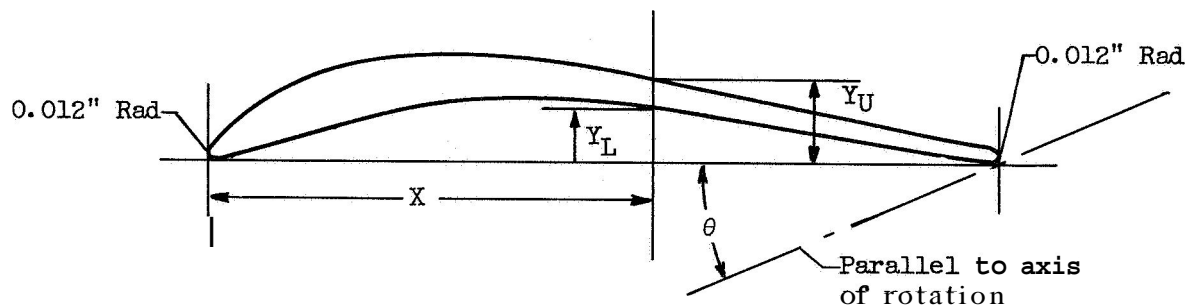


TABLE I. - SURFACE DIFFUSION AND SOLIDITY
PARAMETERS FOR STATOR AND ROTOR BLADES

Blade	Section	Blade-surface diffusion parameters			Solidity, σ
		D_s	D_p	D_{tot}	
Stator	Hub	0.06			1.08
	Mean	.10			1.15
	Tip	.12			3.19
Rotor	Hub	0	0.50	0.50	2.71
	Mean	.10	.43	.53	1.59
	Tip	0	.22	.22	.99

TABLE II. - BLADE-SECTION COORDINATES

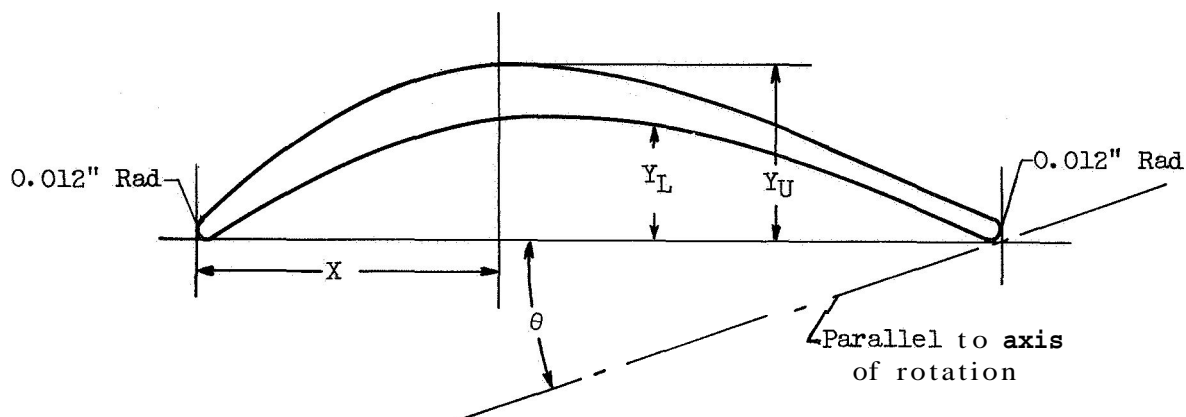
(a) Stator blade



X, in.	Hub		Mean		Tip	
	$e = 48^{\circ}0'$ $r/r_t = 0.533$		$e = 40^{\circ}40'$ $r/r_t = 0.766$		$e = 32^{\circ}42'$ $r/r_t = 1.000$	
	Y_L , in.	Y_U , in.	Y_L , in.	Y_U , in.	Y_L , in.	Y_U , in.
0	0.012	0.012	0.012	0.012	0.012	0.012
.05	.012	.064	.011	.059	.015	.050
.10	.028	.099	.025	.096	.036	.081
.15	.043	.123	.038	.125	.055	.112
.20	.056	.139	.051	.149	.073	.140
.25	.067	.149	.064	.168	.089	.166
.30	.075	.153	.074	.181	.102	.188
.35	.081	.154	.085	.191	.114	.207
.40	.086	.152	.094	.196	.124	.221
.45	.089	.147	.101	.198	.131	.232
.50	.089	.139	.107	.197	.138	.238
.60	.082	.121	.113	.186	.145	.241
.70	.068	.101	.113	.170	.148	.234
.80	.052	.082	.108	.150	.147	.219
.90	.035	.063	.096	.132	.141	.201
1.00	.018	.044	.082	.113	.134	.182
1.10	.000	.024	.066	.095	.123	.162
1.115	.012	.012				
1.20,			.049	.076	.108	.143
1.30			.031	.058	.092	.123
1.40			.014	.040	.075	.103
1.50					.058	.084
1.502			.012	.012		
1.60					.039	.064
1.70					.021	.045
1.802					.012	.012

TABLE II. - Concluded. BLADE-SECTION COORDINATES

(b) Rotor blade



X , in	Hub		Mean		Tip	
	$\theta = -5^{\circ}12'$ $r/r_t = 0.533$		$\theta = 13^{\circ}12'$ $r/r_t = 0.766$		$\theta = 34^{\circ}0'$ $r/r_t = 1.000$	
	Y_L , in.	Y_U , in.	Y_L , in.	Y_U , in.	Y_L , in.	Y_U , in.
0	0.012	0.012	0.012	0.012	0.012	0.012
.1	.070	.121	.052	.105	.015	.069
.2	.138	.215	.104	.175	.026	.098
.3	.194	.290	.140	.223	.036	.112
.4	.236	.342	.164	.245	.043	.112
.5	.264	.373	.173	.243	.046	.105
.6	.278	.384	.169	.231	.045	.092
.7	.276	.376	.153	.202	.040	.078
.8	.261	.347	.126	.165	.035	.063
.9	.231	.300	.090	.120	.024	.049
1.0	.188	.240	.050	.075	.010	.035
1.076					.012	.012
1.1	.132	.170				
1.124			.012	.012		
1.2	.064	.095				
1.302	.012	.012				

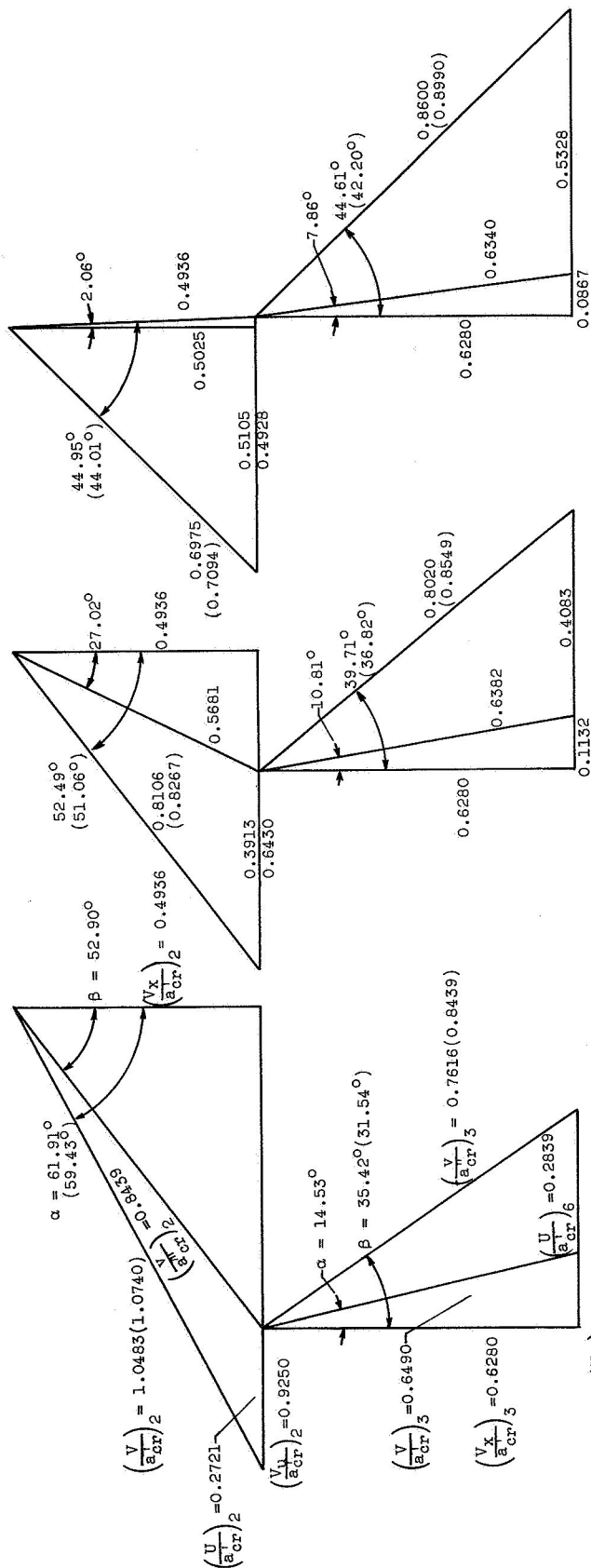
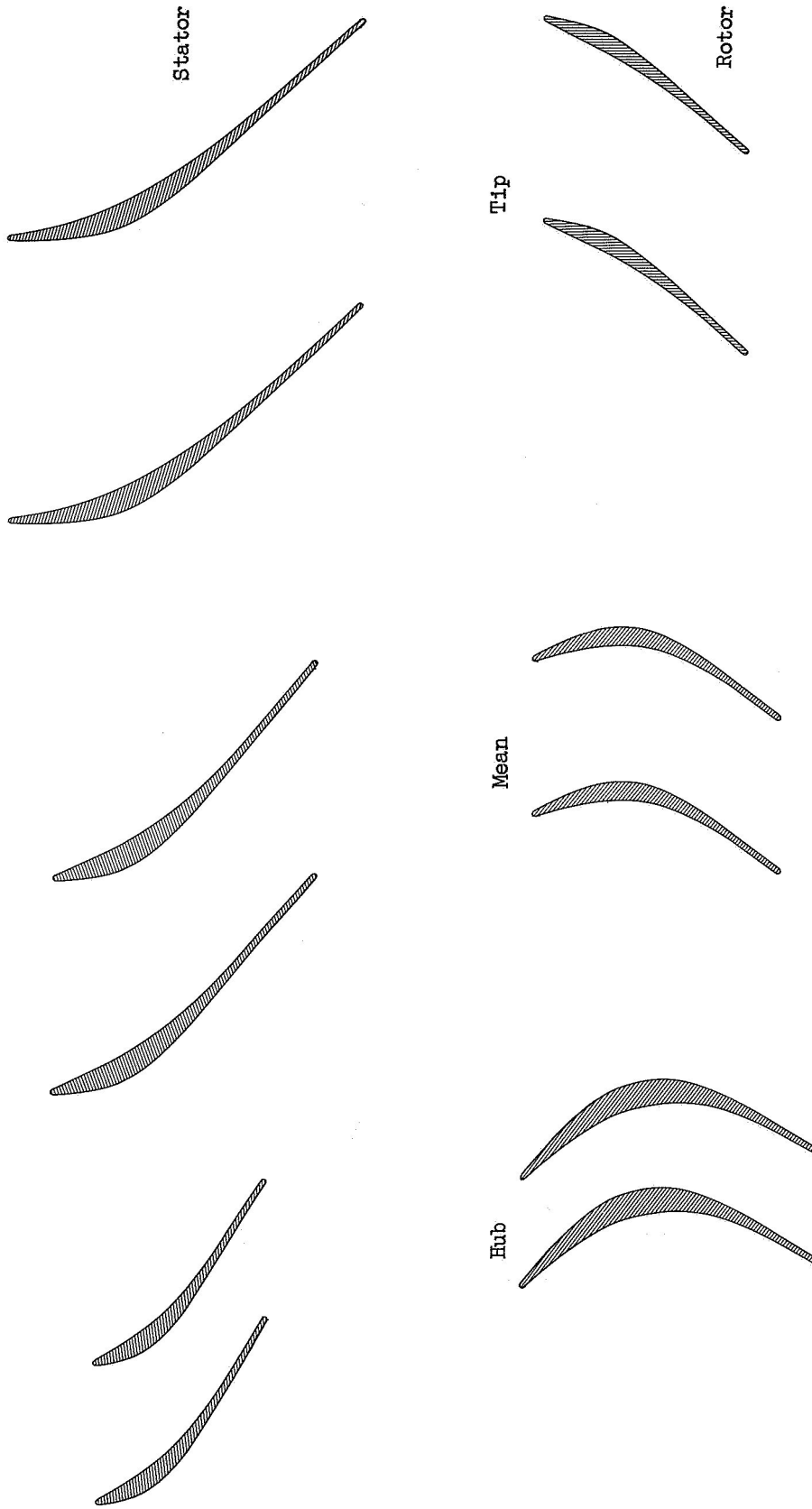


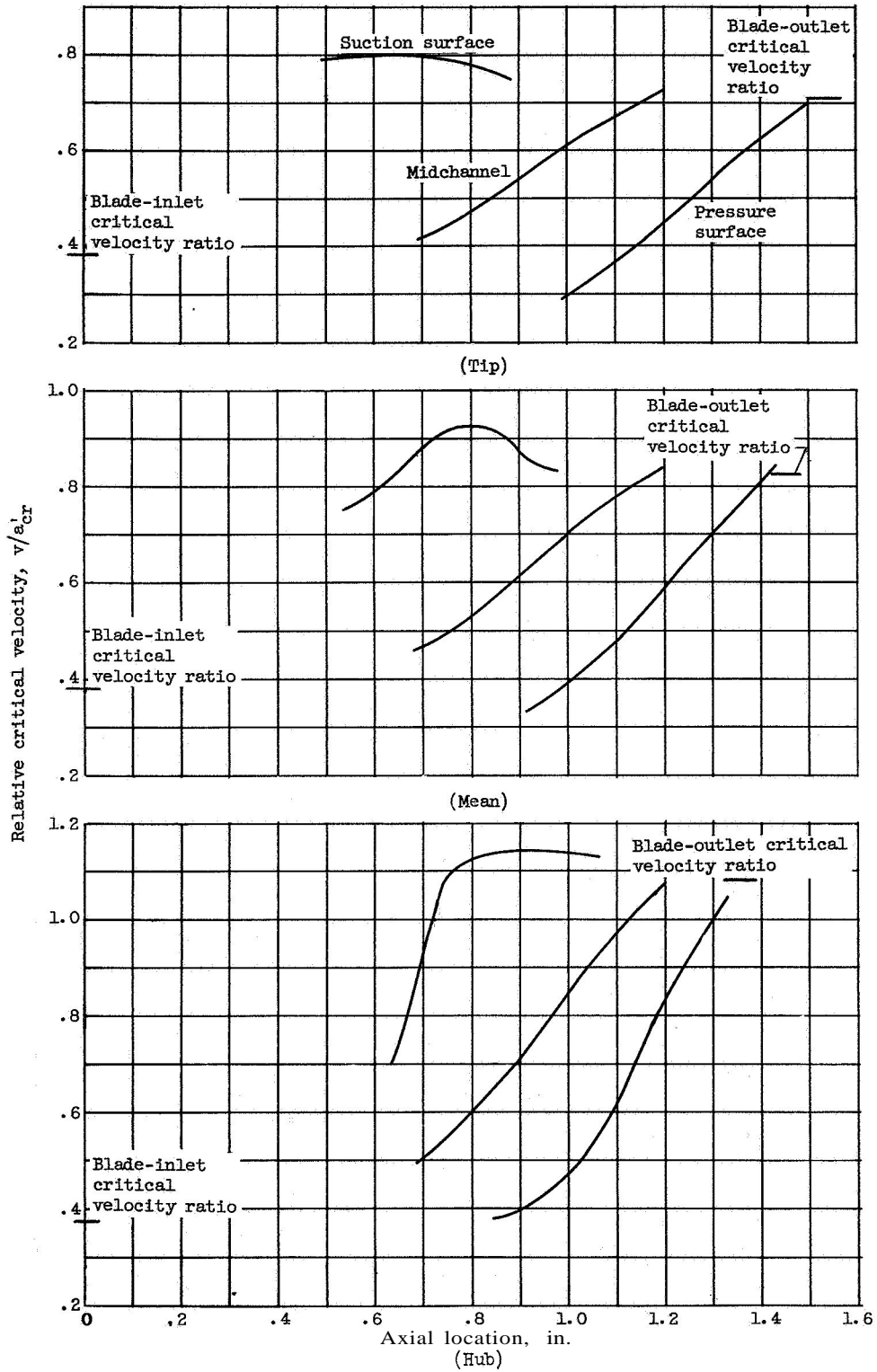
Figure 1. - Definition of angles and side lengths in the plane of the triangle. Mean

SECRET



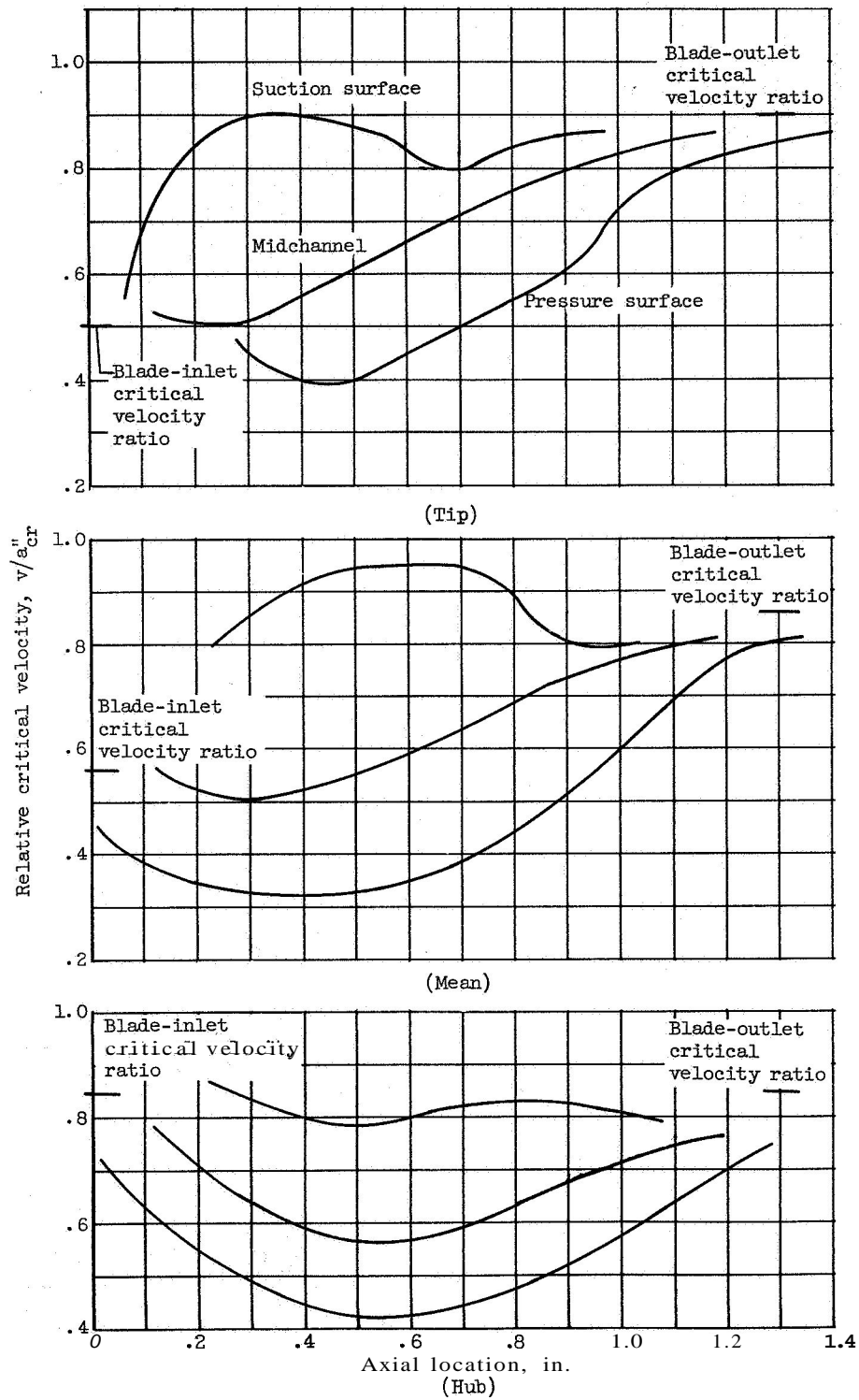
CD-5937

Figure 2 - Stator- and rotor-blade passages and profiles.



(a) Stator blade.

Figure 3 - Design blade midchannel and surface-velocity distribution at hub, mean, and tip sections as a function of axial location.



(b) Rotor blade.

Figure 3. - Concluded. Design blade midchannel and surface-velocity distribution at hub, mean, and tip sections as a function of axial location.

~~CONFIDENTIAL~~

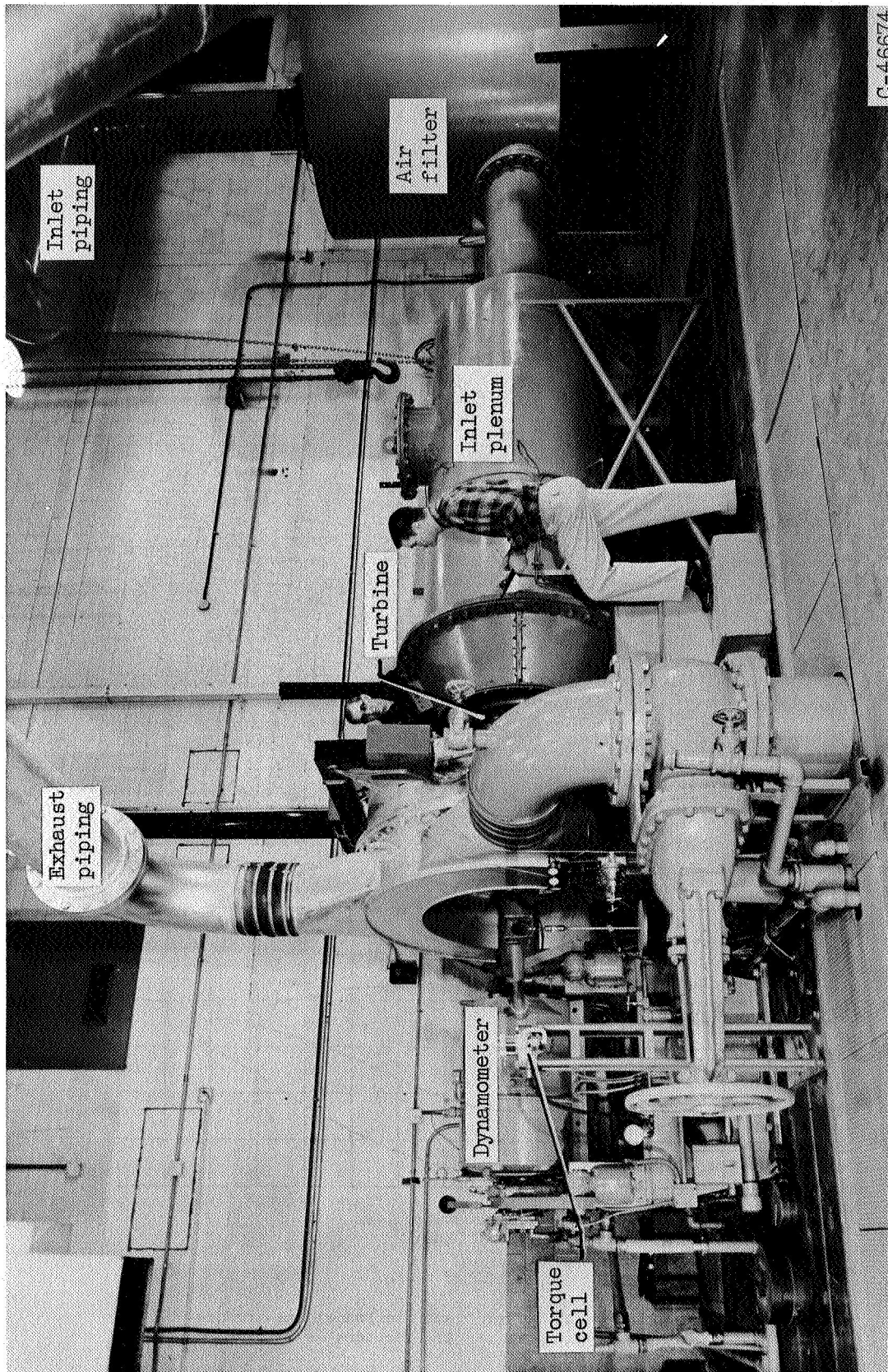
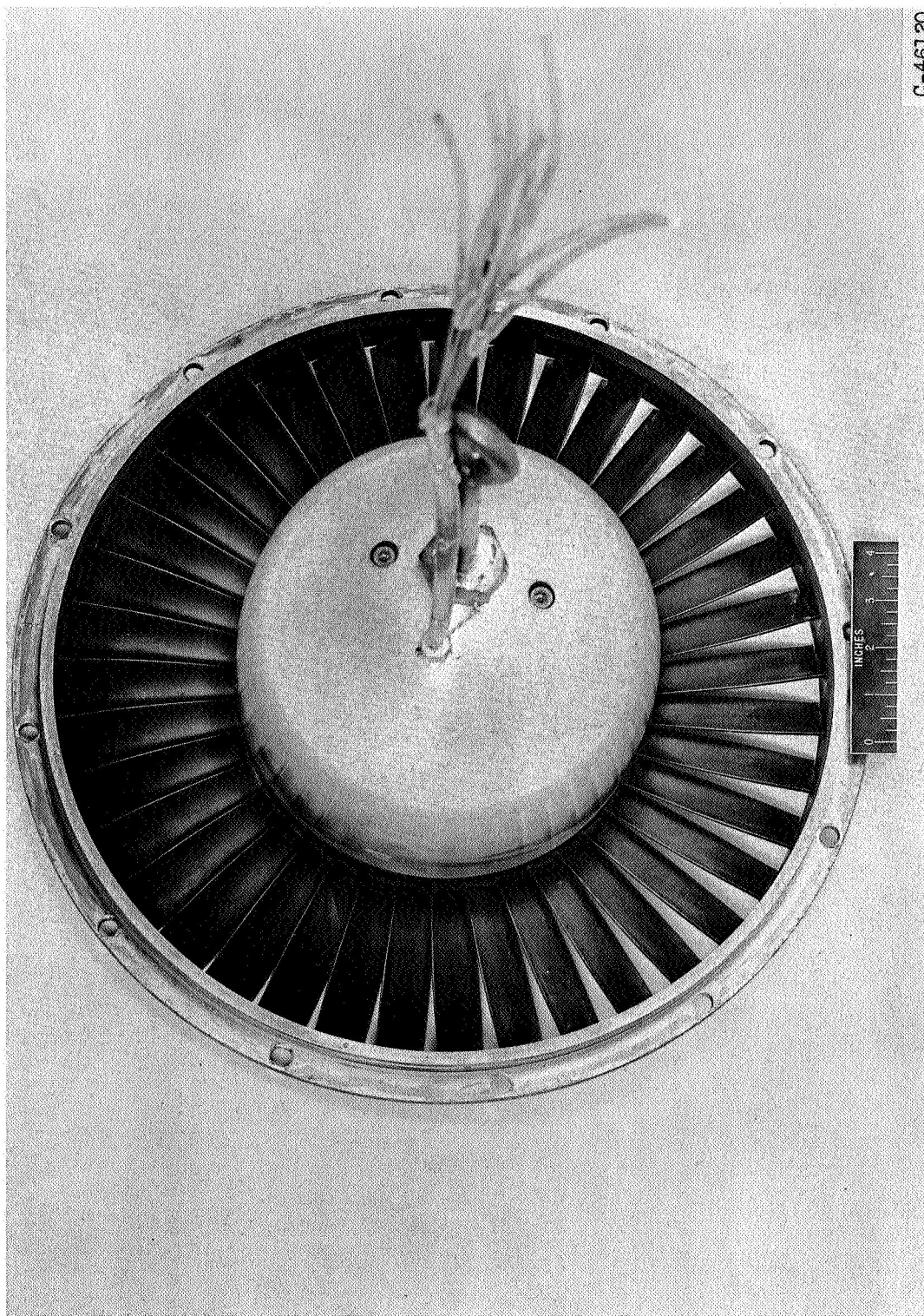
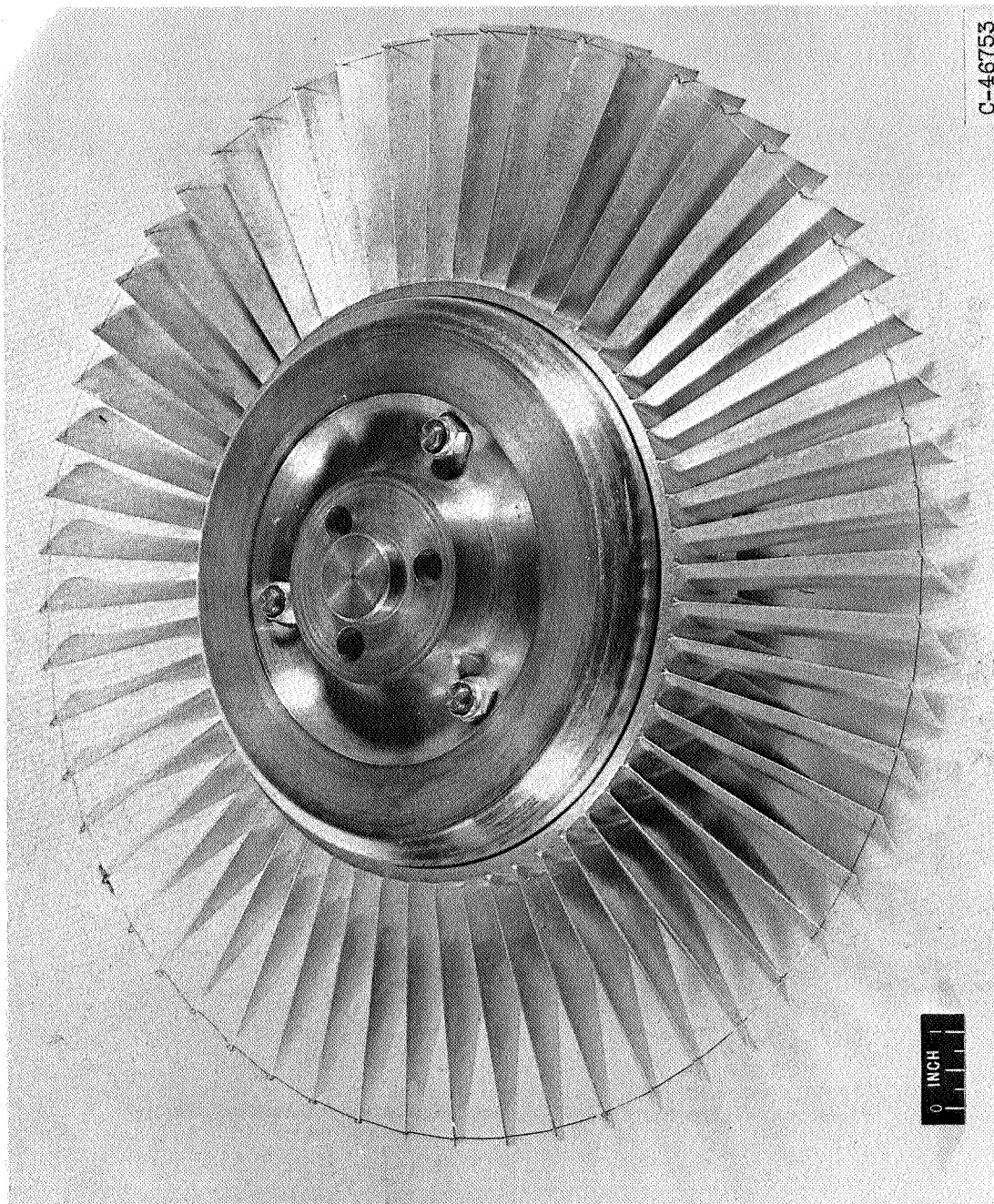


Figure 4. - Installation of turbine in cold air, turbine-component test facility.



(a) Stator-blade assembly.

Figure 5. - Turbine stator and rotor assemblies.



(b) Rotor-blade assembly.

Figure 5 - Concluded. Turbine stator and rotor assemblies

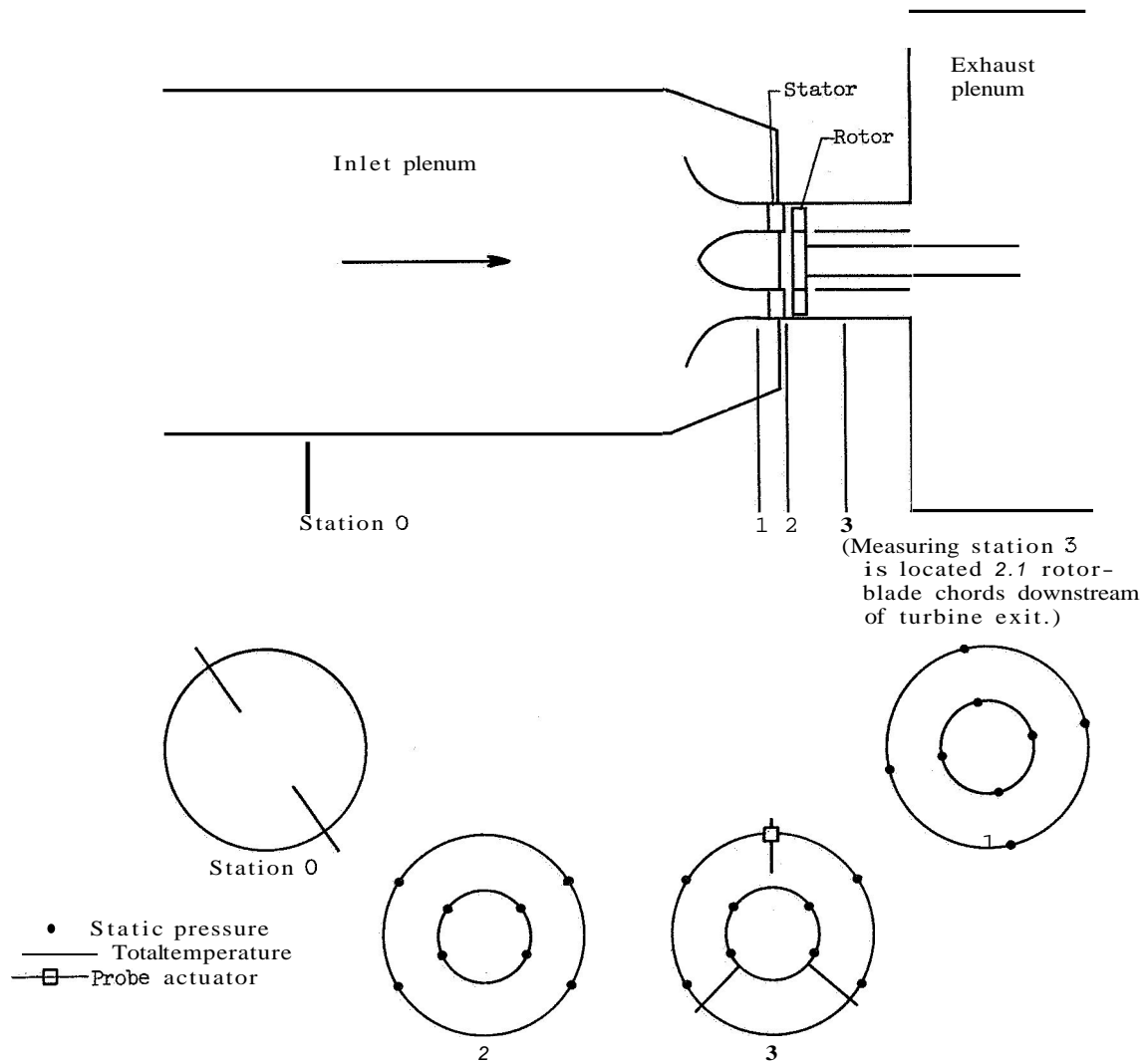
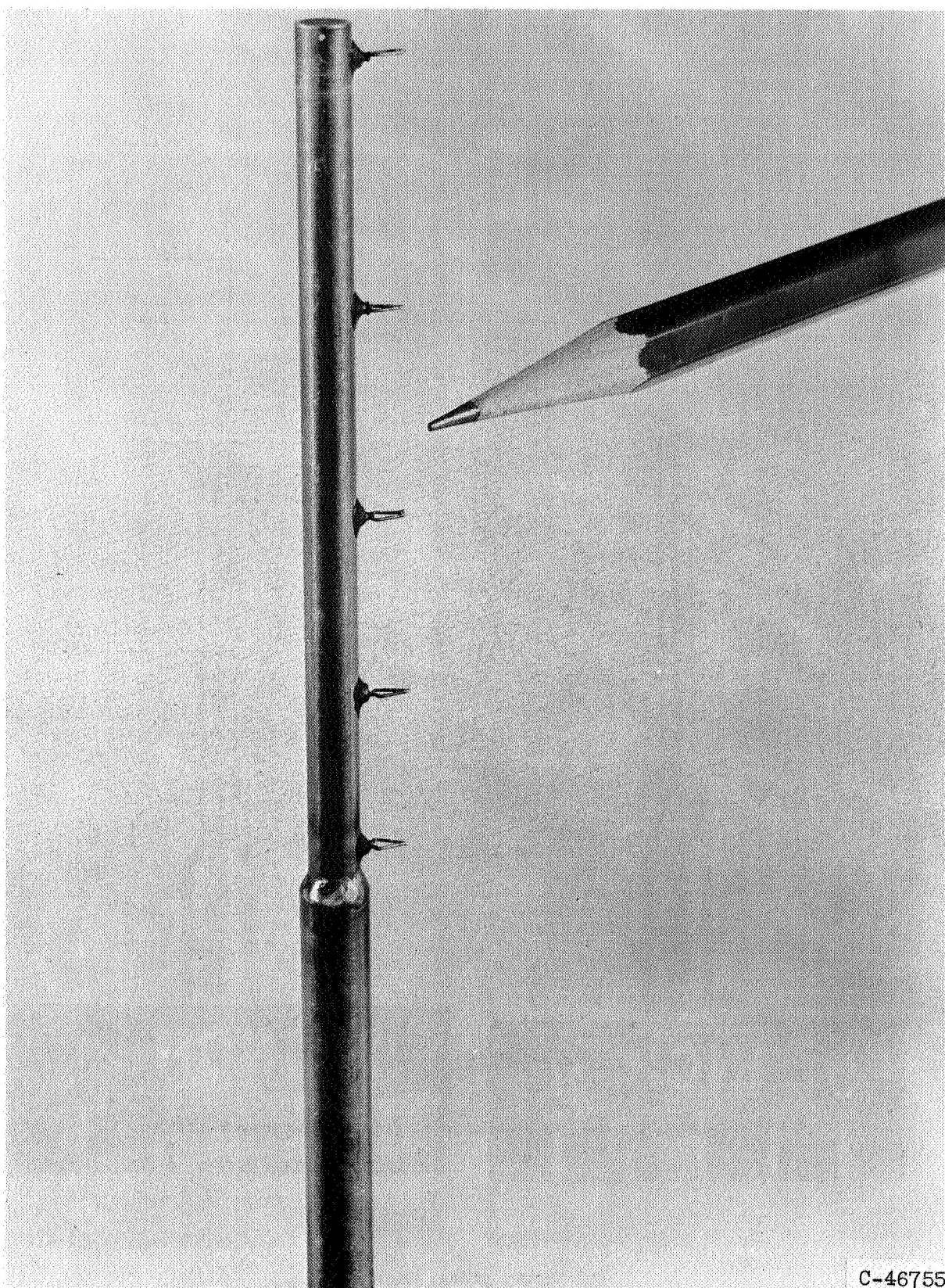


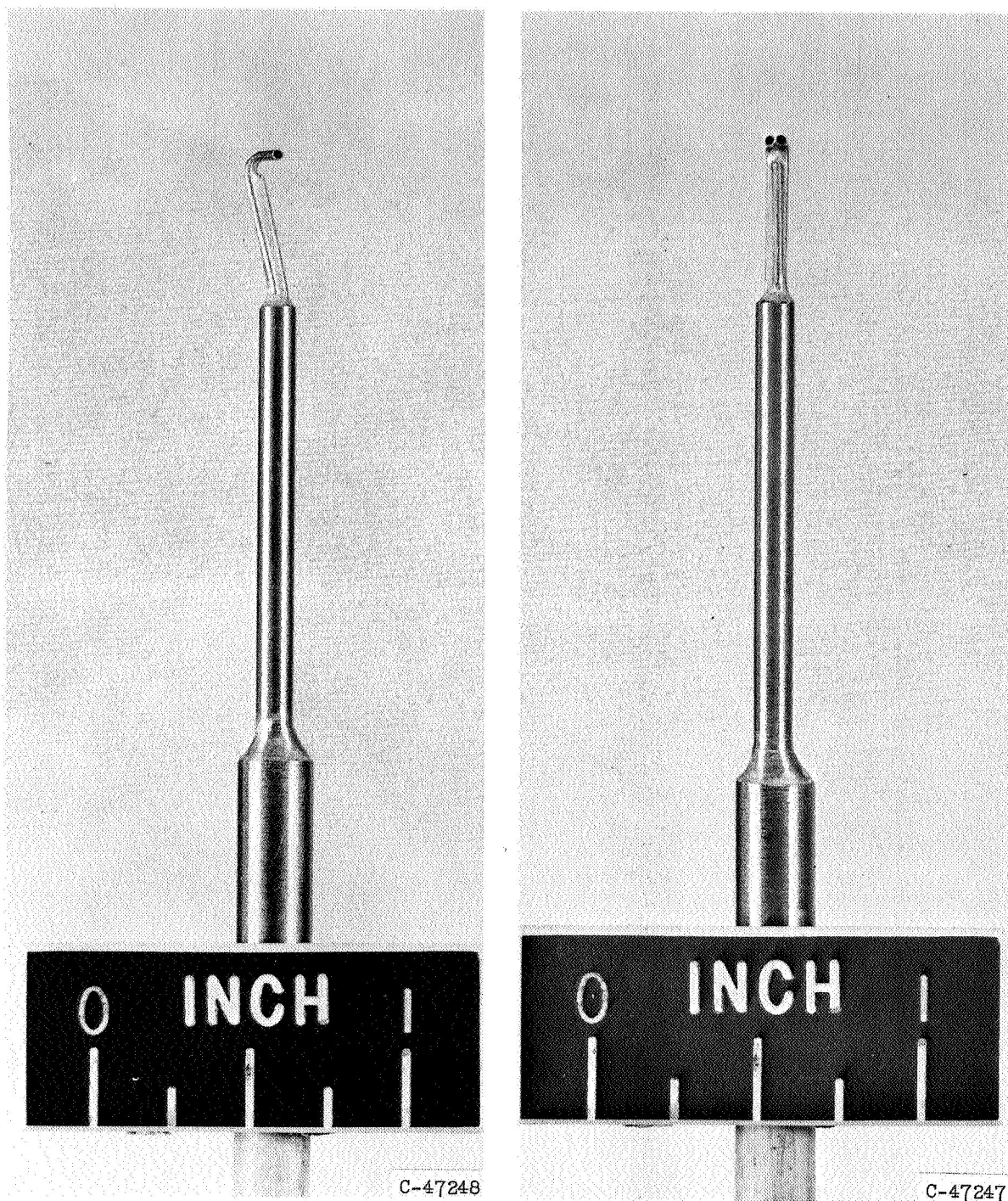
Figure 6. - Schematic diagram of turbine showing instrumentation.



(a) Total-temperature rake.

Figure 7. - Typical instruments.

CONFIDENTIAL

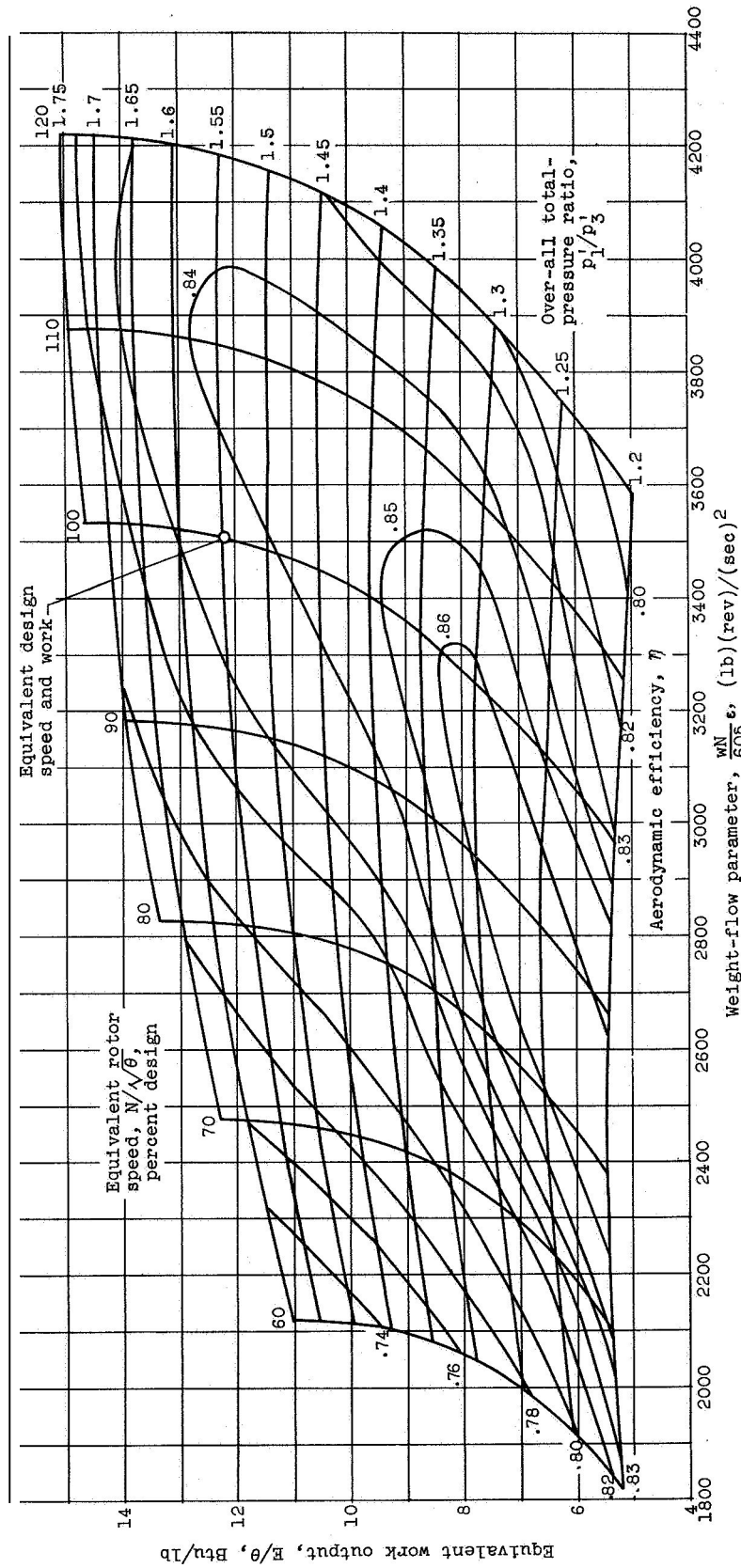


(b) Survey probe, angle.

Figure 7. - Concluded. Typical instruments.



Wigwag 8 - over all 8000000



(b) Aerodynamic efficiency basis.

Figure 8. - Concluded. Over-all performance of turbine.

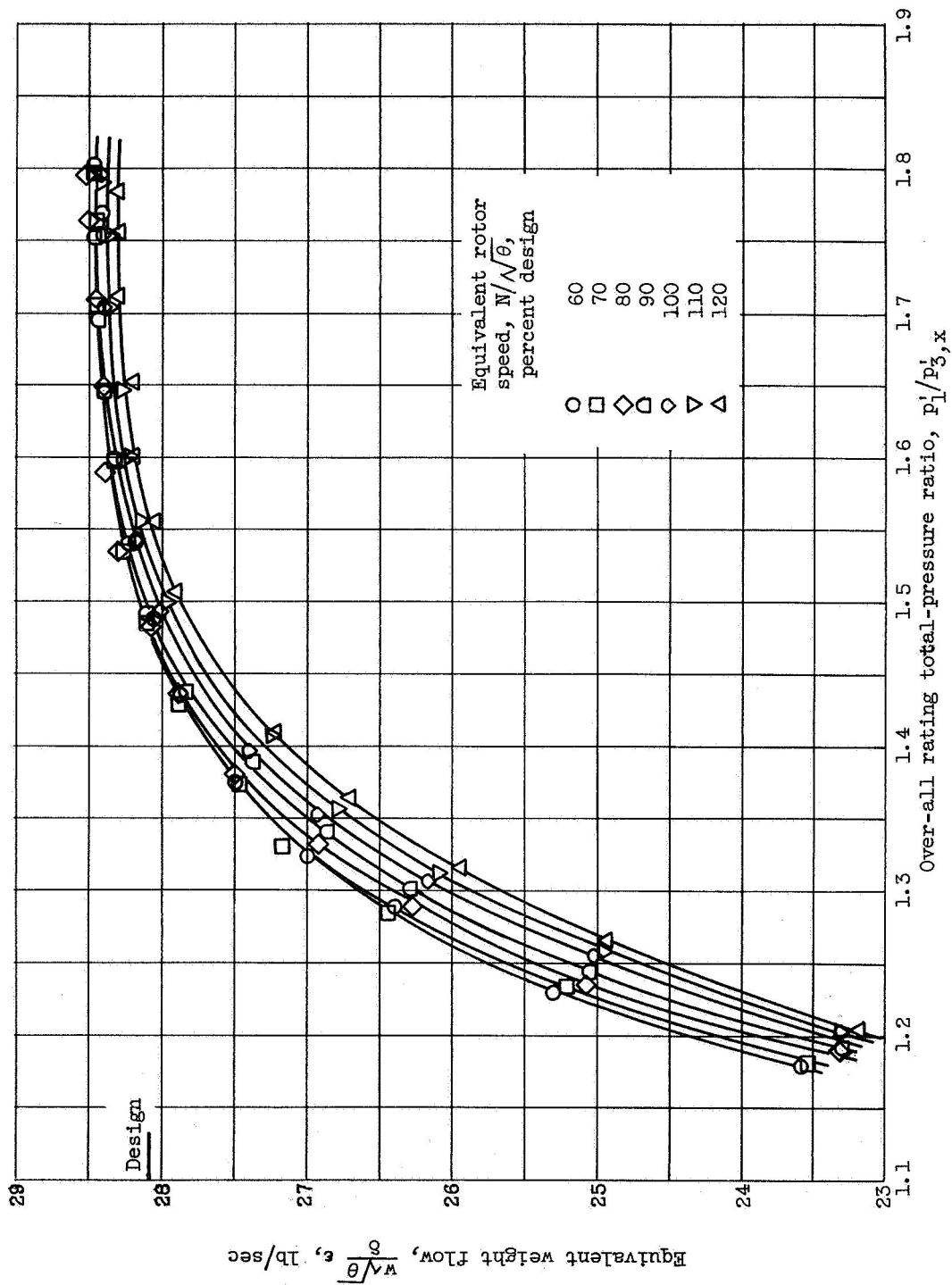


Figure 9. - Variation of equivalent weight flow with rating pressure ratio for values of constant equivalent rotor speed.

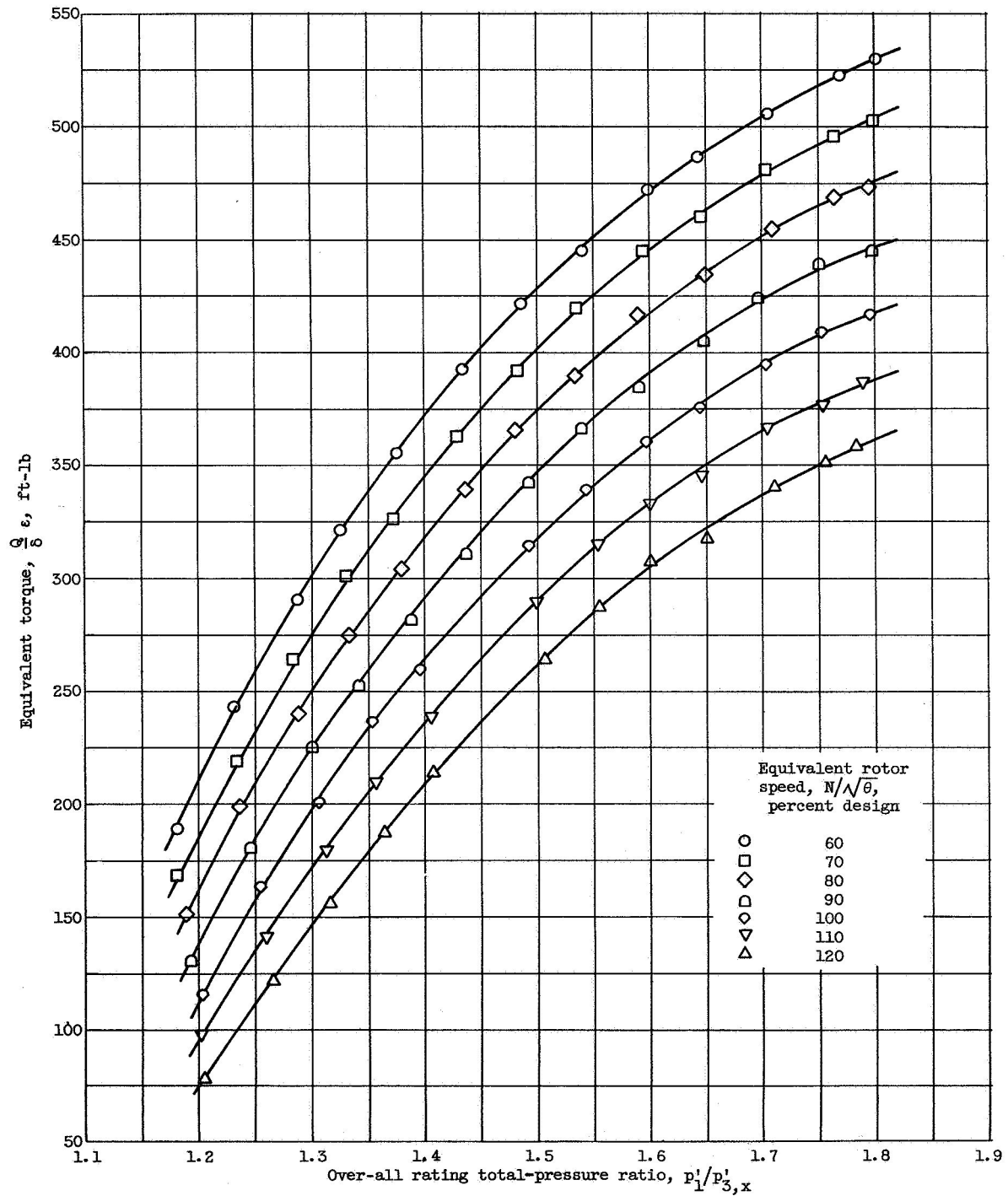


Figure 10. - Variation of equivalent torque with rating total-pressure ratio for values of constant equivalent rotor speed.